A geometry-based stochastic MIMO model for vehicle-to-vehicle communications

Kåredal, Johan; Tufvesson, Fredrik; Czink, Nicolai; Paier, Alexander; Dumard, Charlotte; Zemen, Thomas; Mecklenbräuker, Christoph; Molisch, Andreas

Link to publication

LUND UNIVERSITY

PO Box 117
221 00 Lund
+46 46-222 00 00

A Geometry-Based Stochastic MIMO Model for Vehicle-to-Vehicle Communications

Johan Karedal, *Member, IEEE*, Fredrik Tufvesson, *Senior Member, IEEE*, Nicolai Czink, *Member, IEEE*,
Alexander Paier, *Student Member, IEEE*, Charlotte Dumard, *Member, IEEE*,
Thomas Zemen, *Senior Member, IEEE*, Christoph F. Mecklenbräuker, *Senior Member, IEEE*,
and Andreas F. Molisch, *Fellow, IEEE*

Abstract—Vehicle-to-vehicle (VTV) wireless communications have many envisioned applications in traffic safety and congestion avoidance, but the development of suitable communications systems and standards requires accurate models for the VTV propagation channel. In this paper, we present a new wideband multiple-input-multiple-output (MIMO) model for VTV channels based on extensive MIMO channel measurements performed at 5.2 GHz in highway and rural environments in Lund, Sweden. The measured channel characteristics, in particular the non-stationarity of the channel statistics, motivate the use of a geometry-based stochastic channel model (GSCM) instead of the classical tapped-delay line model. We introduce generalizations of the generic GSCM approach and techniques for parameterizing it from measurements and find it suitable to distinguish between diffuse and discrete scattering contributions. The time-variant contribution from discrete scatterers is tracked over time and delay using a high resolution algorithm, and our observations motivate their power being modeled as a combination of a (deterministic) distance decay and a slowly varying stochastic process. The paper gives a full parameterization of the channel model and supplies an implementation recipe for simulations. The model is verified by comparison of MIMO antenna correlations derived from the channel model to those obtained directly from the measurements.

Index Terms—Channel measurements, MIMO, vehicular, non-stationary, Doppler, geometrical model, statistical model.

I. INTRODUCTION

IN recent years, vehicle-to-vehicle (VTV) wireless communications have received a lot of attention, because of its numerous applications. For example, sensor-equipped cars that communicate via wireless links and thus build up ad-hoc networks can be used to reduce traffic accidents and facilitate traffic flow [1]. The growing interest in this area is also reflected in the allocation of 75 MHz in the 5.9 GHz band dedicated for short-range communications (DSRC) by the US frequency regulator FCC. Another important step was the development of the IEEE standard 802.11p, Wireless Access in Vehicular Environments (WAVE) [2]. Future developments in the area are expected to include, inter alia, the use of multiple antennas (MIMO), which enhance reliability and capacity of the VTV link [3], [4].

It is well-known that the design of a wireless system requires knowledge about the characteristics of the propagation channel in which the envisioned system will operate. However, up to this point, only few investigations have dealt with the single-antenna VTV channel, and even fewer have considered MIMO VTV channels. Most importantly, there exists, to the author's best knowledge, no current MIMO model fully able to describe the time-varying nature of the VTV channel reported in measurements [5].

In general, there are three fundamental approaches to channel modeling: deterministic, stochastic, and geometry-based stochastic [6], [7]. In a *deterministic* approach, Maxwell's equations (or an approximation thereof) are solved under the boundary conditions imposed by a specific environment. Such a model requires the definition of the location, shape, and electromagnetic properties of objects. Deterministic VTV modeling has been explored extensively by Wiesbeck and co-workers [8], [9], [10], and shown to agree well with (single-antenna) measurements. However, deterministic modeling by its very nature requires intensive computations and makes it difficult to vary parameters; it thus cannot be easily used for extensive system-level simulations of communications systems.

Stochastic channel models provide the statistics of the power received with a certain delay, Doppler shift, angle-of-arrival etc. In particular, the tapped-delay-line model, which is based on the wide-sense stationary uncorrelated scattering (WSSUS) assumption [11], is in widespread use for cellular system simulations [12], [13], [14]. For the VTV channel, a tapped delay-Doppler profile model was developed by Ingram and coworkers [15], [16] and also adopted by the

IEEE 802.11p standards group for its system development [2]. However, as also recognized by Ingram [17] and others, assuming a fixed Doppler spectrum for every delay, does not represent the non-stationary channel responses reported in measurements [5], in other words, the WSSUS assumption is usually violated in VTV channels [18].

Geometry-based stochastic channel models (GSCMs) [19], [20] have previously been found well suited for non-stationary environments [21], [22] and this is the type of model we aim for in this paper. GSCMs build on placing (diffuse or discrete) scatterers at random, according to certain statistical distributions, and assigning them (scattering) properties. Then the signal contributions of the scatterers are determined from a greatly-simplified ray tracing, and finally the total signal is summed up at the receiver. This modeling approach has a number of important benefits: (i) it can easily handle non-WSSUS channels, (ii) it provides not only delay and Doppler spectra, but inherently models the MIMO properties of the channel, (iii) it is possible to easily change the antenna influence, by simply including a different antenna pattern, (iv) the environment can be easily changed, and (v) it is much faster than deterministic ray tracing, since only single (or double) scattering needs to be simulated. A few GSCMs where scatterers are placed on regular shapes around TX and RX have been developed for VTV communication, e.g., two-ring models [23] and two-cylinder models [24]. Such approaches are useful for analytical studies of the joint space-time correlation function since they enable the derivation of closed-form expressions. However, their underlying assumption of all scatterers being static does not agree with results reported in measurements [18]. A more realistic placement of scatterers [22], rather reproducing the physical reality, can remedy this. The drawback compared to regular-shaped models is that closed-form expressions generally cannot be derived, but there is a major advantage in terms of easily reproducing realistic temporal channel variations. In this paper, we present such a model for the VTV channel and parameterize it based on the results from an extensive measurement campaign on highways and rural roads near Lund, Sweden.

The main contributions of this paper are the following:

- We develop a generic modeling approach for VTV channels based on GSCM. In this context, we extend existing GSCM structures by prescribing fading statistics for specific scatterers.
- We develop a high resolution method that allows extracting scatterers from the non-stationary impulse responses, and track the contributions over large distances.
- Based on the extracted scatterer contributions, we parameterize the generic channel model.
- We present a detailed implementation recipe, and verify our parameterized model by comparing MIMO correlation matrices as obtained from our model to those derived from measurements.

The remainder of the paper is organized as follows: Sec. II briefly describes a measurement campaign for vehicle-to-vehicle MIMO channels that serves as the motivation for our modeling approach, Sec. III points out the most important channel characteristics to be included in the model, as well as methods for data analysis. The channel model is described in Sec. IV. First the model is outlined and then its different components are described in detail and parameterized from the measurements. Sec. V gives an implementation recipe for the model, whereas Sec. VI compares simulations of the model to the measurement results it is built upon. Finally, a summary and conclusions in Sec. VII wraps up the paper.

II. A VEHICLE-TO-VEHICLE MEASUREMENT CAMPAIGN

In this section, we describe a recent measurement campaign for MIMO VTV channels that serves as the basis for the development of the channel model, i.e., from which the model structure is motivated and the model parameters are extracted. For space reasons, we only give a brief summary; a more detailed description can be found in [5] and [25].

A. Measurement Setup

VTV channel measurements were performed with the RUSK LUND channel sounder that performs MIMO measurements based on the "switched array" principle [26]. The equipment uses an OFDM-like, multi-tone signal to sound the channel and records the time-variant complex channel transfer function $H(t, f)$. Due to regulatory restrictions as well as limitations in the measurement equipment, a center frequency of 5.2 GHz was selected for the measurements. This band is deemed close enough to the 5.9 GHz band dedicated to VTV communications such that no significant differences in the channel propagation properties are to be expected. The measurement bandwidth, B, was 240 MHz, and a test signal length of 3.2 μs was used, corresponding to a path resolution of 1.25 m and a maximum path delay of 959 m, respectively. The transmitter output power was 0.5 W. Using built-in GPS receivers with a sampling interval of 1 s, the channel sounder also recorded positioning data of transmitter (TX) and receiver (RX) during the measurements.

The time-variant channel was sampled every 0.3072 ms, corresponding to a sampling frequency of 3255 Hz during a time window of roughly 10 s (a total of 32500 channel samples); the time window was constrained by the storage capacity of the receiver. The sampling frequency implies a maximum resolvable Doppler shift of 1.6 kHz, which corresponds to a relative speed of 338 km/h at 5.2 GHz.

TX and RX were mounted on the platforms of separate pickup trucks, both deploying circular antenna arrays at a height of approximately 2.4 m above the street level. Each array consisted of 4 vertically polarized microstrip antenna elements,[1] mounted such that their broadside directions were directed at 45, 135, 225 and 315 degrees, respectively, where 0 degrees denotes the direction of travel (the 3 dB beamwidth was approximately 85 degrees). Thus, a 4×4 MIMO system was measured.

B. Measured Traffic Environments

We performed measurements in two different environments: a rural motorway (Ru) and a highway section (Hi), both located near Lund, Sweden. The rural surroundings, a one-lane motorway located just north of Lund, are mainly characterized by fields on either side of the road, with some residential

---

[1]More precisely, on each array a subset of 4 elements out of a total of 32 was selected evenly spaced along the perimeter.

houses, farm houses and road signs sparsely scattered along the roadside. Little to no traffic prevailed during these measurements.

The surroundings of the two-lane highway can be best described as rural or suburban, despite being within the Lund city limits. Large portions of the roadside consist of fields or embankments; the latter constituting a noise barrier for residential areas.[2] Some road signs and a few low-rise commercial buildings are located along the roadside, but with the exception of the areas near the exit ramps, strong *static* scattering points are anticipated to be scarce along the measurement route. Measurements were taken during hours with little to medium traffic density; the road strip had an average of 33000–38000 cars per 24 hours during 2006 [27].

Measurements were performed both with TX and RX driving in the same direction (SM), and with TX and RX driving in opposite directions (OP). During each measurement, the aim was to maintain the same speed for TX and RX, though this speed was varied between different measurements in order to obtain a larger statistical ensemble. Also, the distance between TX and RX was kept approximately constant during each SM measurement, though it varied between different measurements. 32 SM and 12 OP measurements were performed in the rural scenario, whereas 19 SM and 21 OP measurements were performed in the highway scenario.

III. VTV CHANNEL CHARACTERISTICS

In this section we analyze some measurement results in order to draw conclusions about the fundamental propagation mechanisms of the VTV channel. Since any channel model is a compromise between simplicity and accuracy, our goal is to construct a model that is simple enough to be tractable from an implementation point of view, yet still able to emulate the essential VTV channel characteristics. For space reasons, our discussions are rather brief; more results as well as discussions can be found in [5] and [25].

A. Time-Delay Domain

By Inverse Discrete Fourier Transforming (IDFT) the recorded frequency responses $H(t, f)$, using a Hanning window to suppress side lobes, we obtain complex channel impulse responses $h(t, \tau)$. The influence of small-scale fading is removed by averaging $|h(t, \tau)|^2$ over a sample time corresponding to a TX movement of 20 wavelengths, λ, resulting in average power delay profiles (APDPs).

Fig. 1 shows a typical sample plot of the time-variant APDP for a highway measurement. In this measurement, TX and RX were driving in the same direction at a speed of 110 km/h, separated by slightly more than 100 m, and the figure shows the antenna subchannel where both elements have their main lobes directed at 315 degrees. From the time-delay domain results, we draw the following conclusions: (i) the LOS path is always strong, (ii) significant energy is available through discrete components, typically represented by a single tap (e.g., the two components near 0.8 μs propagation delay in Fig. 1), (iii) discrete components typically move through many delay bins during a measurement; this implies that

---

2Such arrangements are common for European cities.
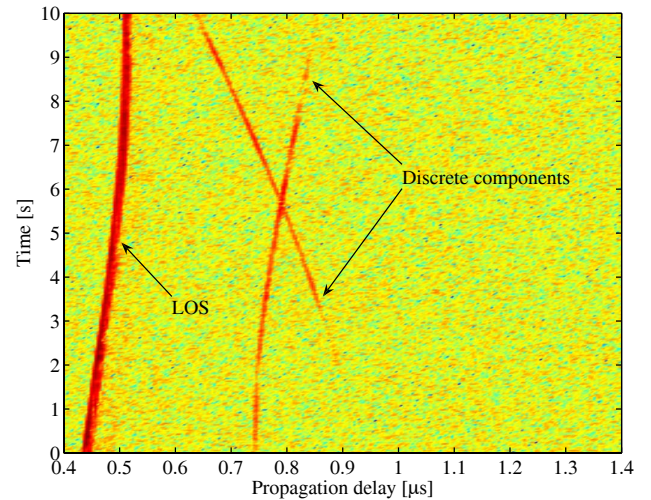
Fig. 1. Example plot of the time-varying APDP of a highway SM measurement with an approximate TX/RX speed of 110 km/h. The antenna channel in question uses elements directed at 315 degrees, i.e., close to opposite the direction of travel. The reflections from two discrete scatterers, both cars following the TX/RX, are clearly visible in the figure.
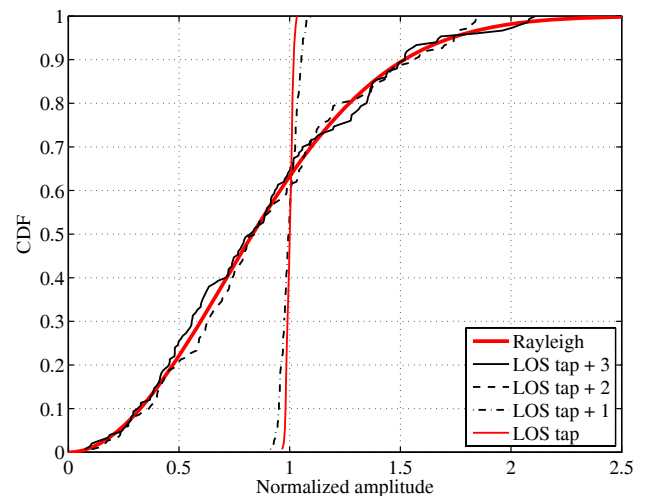
Fig. 2. Example plot of the small-scale amplitude statistics for taps immediately following the LOS tap. The figure shows the result derived from the 150 first temporal samples (corresponding to 5 ms or a TX/RX movement of 20 wavelengths) of a highway SM measurement with a TX/RX speed of 90 km/h.

the common assumption of WSSUS is violated, (iv) discrete components may stem from mobile as well as static scattering objects, and (v) the LOS is usually followed by a tail of weaker components. Analyzing the amplitude statistics of the taps immediately following the LOS tap shows that they can be well described by a Rayleigh distribution (see Fig. 2).

The recorded GPS-coordinates of the TX and RX units can be used in conjunction with the time-delay domain results. By using GPS coordinates of known objects along the measurement route, such as buildings, bridges and road signs, we can compute the theoretical time-varying propagation distance from TX to scatterer to RX, and compare it to the occurrence of discrete reflections in the time-delay domain. This way we can associate physical objects with contributions in the time-variant APDP.
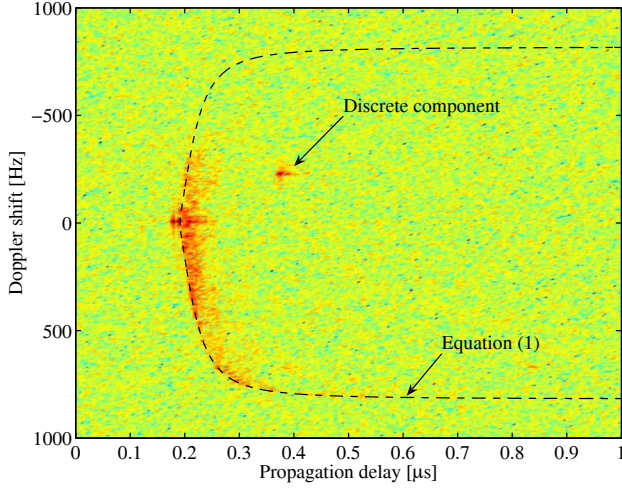
Fig. 3. Example plot of the Doppler-resolved impulse response of a highway SM measurement (though different to the one in Fig. 1), derived over a time interval of 0.15 s. A discrete component is visible at approximately 0.4 μs propagation delay. Also plotted in the figure is the Doppler shift vs. distance as produced by (1), i.e., for scatterers located on a line parallel to (and a distance 5 m away from) the TX/RX direction of motion.

B. Delay-Doppler Domain

To investigate the Doppler characteristics of the received signal, Doppler-resolved impulse responses, $h(\nu, \tau)$, were derived by Fourier transforming $h(t, \tau)$ with respect to t; an example is shown in Fig. 3. We draw the following conclusions: (i) the total Doppler spectrum can change significantly during a measurement, as scatterers change their position and speed relative to TX and RX, (ii) the Doppler spread of discrete scatterers is typically small, (iii) the tail of weaker components not only has a large delay spread, but also a large Doppler spread. In the sequel, we denote this part of the channel "diffuse" in order to distinguish it from the discrete components.

For a single-reflection process, simple geometric relations provides the relationship between angles of arrival/departure and scatterer velocity and thus can tell us whether a scatterer is mobile or static. The Doppler shift for a signal propagating from TX to RX, traveling in parallel at speeds v_T and v_R, respectively, via a single bounce off a scatterer traveling in parallel to the TX/RX at a speed v_p, can be expressed as

$$\nu\left(\Omega_{T,p}, \Omega_{R,p}\right) = \frac{1}{\lambda}\left[(v_T - v_p)\cos\Omega_{T,p} + (v_R - v_p)\cos\Omega_{R,p}\right], \quad (1)$$

if the direction-of-arrival $\Omega_{R,p}$ and the direction-of-departure $\Omega_{T,p}$ are given relative to the direction of travel. We find that for $v_p = 0$, the Doppler shift produced by scattering points on a line parallel to the direction of travel closely matches the Doppler characteristics of the tail of diffuse components (see Fig. 3). Our conclusion is thus that proper delay as well as Doppler characteristics of the diffuse tail can be obtained by placing scatterers along the roadside.

C. Tracking a Discrete Scatterer

Further insights can be gained by looking at the time-varying signal contribution of each discrete scatterer, such as

the two distinct paths of Fig. 1. We thus need a tool to track the signal over time. One way of doing so would be to assume an underlying physical propagation model based on the exact locations of TX, RX and each scatterer, and determine the best-fit between model and measurement. However, such an approach is sensitive to model assumptions, as well as uncertainties in the measurements (more specifically in the GPS data).

For those reasons we choose a different approach. We first estimate the delays τ_i and amplitudes α_i of the multipath contributions at each time instant separately, and then perform a tracking of the components over large time scales. The first part of this algorithm is achieved by means of a high-resolution approach that is based on a serial "search-and-subtract" of the contributions from the individual scatterers (this is similar to the CLEAN method [28]). We now describe the detailed steps of the algorithm. Define the vectors

$$\mathbf{h}_t = \mathbf{h}(t) = [H_t(f_0) \ldots H_t(f_{N-1})]^T, \quad (2)$$

$$\mathbf{p}(\tau) = \left[\mathrm{e}^{j2\pi f_0 \tau} \ldots \mathrm{e}^{j2\pi f_{N-1}\tau}\right]^T, \quad (3)$$

where $\mathbf{h}_t$ contains the measurement data sampled at time instant t at the frequencies $f_0 \ldots f_{N-1}$ and $\mathbf{p}(\tau)$ is a vector of complex exponentials that is the same for all t. Furthermore, we introduce and initialize an auxiliary vector $\tilde{\mathbf{h}}_t(1) := \mathbf{h}_t$.

The search-and-subtract algorithm is carried out as an iteration of two steps, starting by setting the iteration counter $l = 1$. In the first step, we find the delay[3] corresponding to the component of maximum power in $\tilde{\mathbf{h}}_t(l)$, i.e.,

$$\hat{\tau}(l) = \arg\max_{\tau}\left|\mathbf{p}^T(\tau)\tilde{\mathbf{h}}_t(l)\right|^2, \quad (4)$$

where $(\cdot)^T$ denotes the matrix transpose, and then find the corresponding complex amplitude at $\hat{\tau}(l)$ by

$$\hat{\alpha}(l) = \frac{\mathbf{p}^T(\hat{\tau}(l))\tilde{\mathbf{h}}_t(l)}{\mathbf{p}^T\mathbf{p}}. \quad (5)$$

In the second step, we subtract the contribution of $\{\hat{\alpha}(l), \hat{\tau}(l)\}$ from the measurement data by

$$\tilde{\mathbf{h}}_t(l+1) := \tilde{\mathbf{h}}_t(l) - \hat{\alpha}(l)\mathbf{p}(\hat{\tau}(l)). \quad (6)$$

The algorithm increases the iteration counter to $l := l+1$ and repeats from the first step until $l = L$, where L, the number of multipath components, was set to 20 in our evaluations. For every time instant m, the delay and amplitude estimates are written as a row in the matrices $\hat{\mathbf{T}} \in \mathbb{R}^{M \times L}$ and $\hat{\mathbf{A}} \in \mathbb{C}^{M \times L}$, respectively, where $M = 32500$ and $L = 20$.

Since this method works only on the impulse response for a given time instant, it might mistakenly include noise peaks as multipath components; however, those will be filtered out by the tracking procedure described below. There is thus no requirement to perform aggressive thresholding of the individual impulse responses (such thresholding has undesired consequences like eliminating multipath components with low power).

To track the time-varying delay and power of a reflected path through the matrices $\hat{\mathbf{T}}$ and $\hat{\mathbf{A}}$, we use an algorithm with the following steps:

---

[3]Note that the delay resolution achieved in this search step is better than that of a simple IDFT-based estimate.

Step 1: Find the row m_m and column l_m of the strongest remaining component in $\hat{\mathbf{A}}$ by

$$\{m_m, l_m\} = \arg\max_{m,l} \left| \hat{\mathbf{A}}(m,l) \right|.$$

The corresponding delay estimate of this component is $\hat{\mathbf{T}}(m_m, l_m)$.

Step 2: Look in the adjacent rows (time samples) of $\hat{\mathbf{T}}$, $m_m - 1$ and $m_m + 1$, and find the column *indices* of the "closest" components in these rows, i.e.,

$$l_{m-1} = \arg\min_l \left| \hat{\mathbf{T}}(m_m - 1, :) - \hat{\mathbf{T}}(m_m, l_m) \right|,$$

$$l_{m+1} = \arg\min_l \left| \hat{\mathbf{T}}(m_m + 1, :) - \hat{\mathbf{T}}(m_m, l_m) \right|,$$

where $\hat{\mathbf{T}}(m_m \pm 1, :)$ defines the $(m_m \pm 1)$:th row of $\hat{\mathbf{T}}$, and determine

$$\epsilon_{m-1} = \left| \hat{\mathbf{T}}(m_m - 1, l_{m-1}) - \hat{\mathbf{T}}(m_m, l_m) \right|,$$

$$\epsilon_{m+1} = \left| \hat{\mathbf{T}}(m_m + 1, l_{m+1}) - \hat{\mathbf{T}}(m_m, l_m) \right|.$$

If neither ϵ_{m-1} nor ϵ_{m+1} are $\leq 1/2B$, discard the component in $\{m_m, l_m\}$ by setting $\hat{\mathbf{T}}(m_m, l_m) = \hat{\mathbf{A}}(m_m, l_m) = 0$ and return to step 1.[4] Otherwise, store $\hat{\mathbf{T}}(m_m - 1, l_{m-1})$ and/or $\hat{\mathbf{T}}(m_m + 1, l_{m+1})$ and proceed.

Step 3: Estimate the direction of the samples found so far by fitting a regression line

$$\tilde{\tau}(m) = a + bm \qquad (7)$$

to $\hat{\mathbf{T}}(m_m - 1 \dots m_m + 1, l_{m-1} \dots l_{m+1})$ (given that both samples were stored in the previous step). Then, find $\hat{\mathbf{T}}(m_m - 2, l_{m-2})$ and $\tau(m_m + 2, l_{m+2})$ where

$$l_{m\pm2} = \arg\min_l \left| \hat{\mathbf{T}}(m_m \pm 2, :) - \tilde{\tau}(m_m \pm 2) \right|$$

and determine

$$\epsilon_{m\pm2} = \left| \hat{\mathbf{T}}(m_m \pm 2, l_{m\pm2}) - \tilde{\tau}(m_m \pm 2) \right|.$$

If ϵ_{m-2}, ϵ_{m+2} are $\leq 1/2B$, store $\hat{\mathbf{T}}(m_m - 2, l_{m-2})$ and/or $\hat{\mathbf{T}}(m_m + 2, l_{m+2})$ and repeat this step until neither ϵ_{m-2} nor ϵ_{m+2} are $\leq 1/2B$. Since the curvature of the tracked path may change over time, use at most the N_d last (or N_d first, depending on direction) stored components when determining $\tilde{\tau}$ from (7) in the iterative process.

Step 4: To cope with small temporal "gaps," i.e., situations where the components of a path are missing in one or a few consecutive time bins, search along $\tilde{\tau}$ at both ends for an additional N_{gap} time bins; return to step 3 if a sample is found. Proceed to step 5 when there are "gaps" larger than N_{gap} at both ends.

Step 5: Store the amplitudes in $\hat{\mathbf{A}}$ that correspond to the tracked components in $\hat{\mathbf{T}}$, then remove the tracked components from $\hat{\mathbf{A}}$ and $\hat{\mathbf{T}}$ by setting the appropriate entries to 0. Measure the length, in terms of time bins, of the tracked path. Save only paths larger than N_L time bins; paths shorter than that
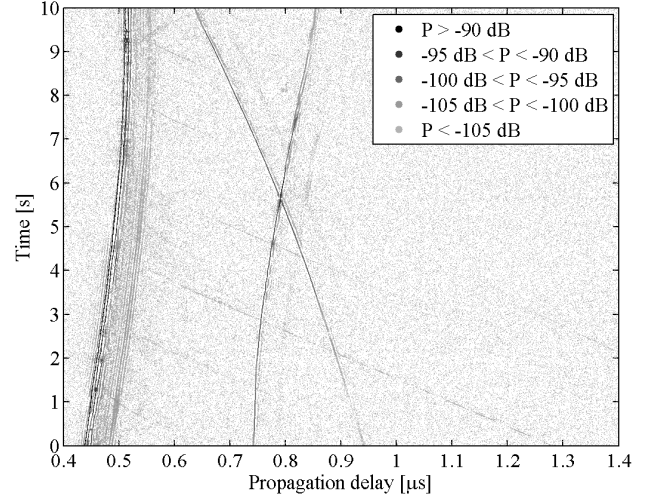

Fig. 4. High resolution impulse response of the measurement in Fig. 1.

are deemed not part of a discrete reflection and discarded. If a stopping criterion, either in terms of residual power in $\hat{\mathbf{A}}$, or in a maximum number of tracked paths, is met, proceed to step 6, otherwise return to step 1.

Step 6: To cope with larger temporal "gaps" (due to a longer time period of path invisibility), estimate $\tilde{\tau}_{p,e}$ and $\tilde{\tau}_{p,b}$ as the start and end extrapolation, respectively, of each path p from (7). Let the row and column indices where p begin and end be $\{m_{p,b}, l_{p,b}\}$ and $\{m_{p,e}, l_{p,e}\}$, respectively, and find the path q that minimizes

$$\begin{aligned} J &= \left| \hat{\mathbf{T}}(m_{p,b}, l_{p,b}) - \tilde{\tau}_{q,e}(m_{p,b}) \right| \\ &\quad + \left| \hat{\mathbf{T}}(m_{q,e}, l_{q,e}) - \tilde{\tau}_{p,b}(m_{q,e}) \right| \\ &= J_1(q,p) + J_2(p,q). \end{aligned}$$

Step 7: If both $J_1(q,p) \leq 1/B$ and $J_2(p,q) \leq 1/B$, combine paths p and q into one and return to step 6. If not, terminate.

The choices for N_d, N_{gap} and N_L have to be done on a rather arbitrary basis; in this analysis, we selected $N_d = 40$ wavelengths, $N_{gap} = 5$ wavelengths and $N_L = 40$ wavelengths.

Fig. 4 shows the outcome of the search-and-subtract algorithm, executed on the measurement in Fig. 1. A drawback of the search-and-subtract approach is visible; any inaccuracy of the underlying model can lead to error propagation. For example, our evaluation assumes an antenna frequency response that is completely flat over the measurement bandwidth; the actual frequency response varies on the order of a few dB. The subtraction thus induces an error seen as "ringing" components, especially around the LOS. However, we also find that the "ringing" or "ghost" components are much weaker than the true components they are surrounding, and thus can be neglected for most practical purposes.[5]

Fig. 5 shows the outcome of the tracking algorithm, where we especially observe the paths, denoted "19" and "25," we saw already in Fig. 1. The power of the tracked signal from the path denoted "19" is shown in Fig. 6. Our general conclusion

---

[4]Note that we are making the implicit assumption that the delay of a component does not change more than $1/B$, where B is the measurement bandwidth, between any two consecutive time bins. This is an eminently reasonable assumption since the channel was sampled every 0.3072 ms and the maximum speed of any involved vehicle is approximately 150 km/h.

[5]Attempts to equalize the antenna frequency response could lead to noise enhancement and thus might not benefit the overall accuracy of the results.
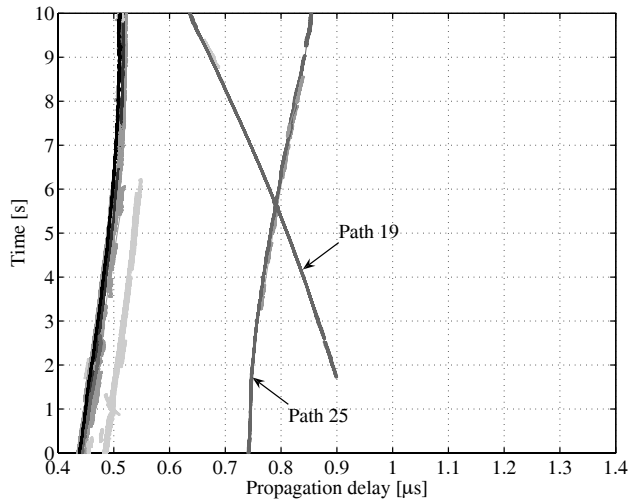
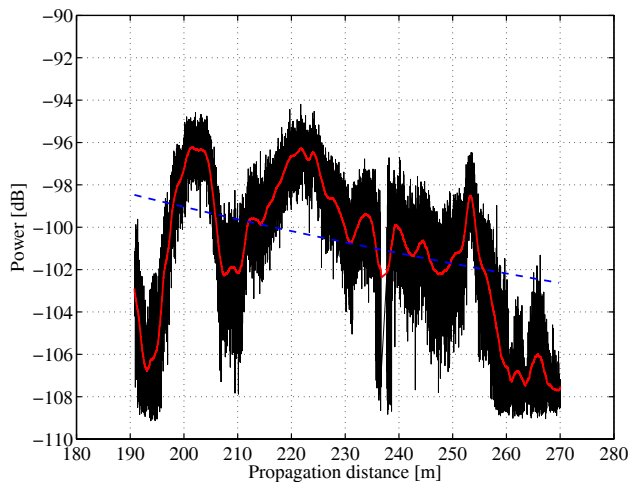Fig. 5. Extracted paths from Fig. 4 as given by the tracking algorithm.

Fig. 6. Extracted power as a function of propagation distance for the path denoted "19" in Fig. 5. The figure also shows estimated distance decay (dashed) and the low-pass filtered signal (red).

from the tracked paths is thus that the signal from a discrete scatterer is time-variant, likely due to inclusion of one or several ground reflections in the total signal. Thus, the standard GSCM way of modeling the complex path amplitudes as non-fading is not well suited for this type of reflections.

IV. A GEOMETRY-BASED STOCHASTIC MIMO MODEL

We are now ready to define our model. First, we give a general model outline, then we go through its parts in detail and describe how they are extracted from the measurement data. Finally, we give the full set of model parameters.

A. General Model Outline

As mentioned in the introduction, the basic idea of GSCMs is to place an ensemble of point scatterers according to a statistical distribution, assign them different channel properties, determine their respective signal contribution and finally sum up the total contribution at the receiver. We therefore define a two-dimensional geometry as in Fig. 7, where we distinguish

between three types of point scatterers: mobile discrete, static discrete, and diffuse.

We model the double-directional, time-variant, complex impulse response of the channel as the superposition of N paths (contributions from scatterers) by [22]

$$h(t, \tau) = \sum_{i=1}^{N} a_i e^{jkd_i(t)} \delta(\tau - \tau_i)$$
$$\times \delta(\Omega_R - \Omega_{R,i})\delta(\Omega_T - \Omega_{T,i})g_R(\Omega_R)g_T(\Omega_T), \quad (8)$$

where τ_i, $\Omega_{R,i}$ and $\Omega_{T,i}$ are the excess delay, angle-of-arrival (AOA), and angle-of-departure (AOD) of path i, $g_T(\Omega_T)$ and $g_R(\Omega_R)$ are the TX and RX antenna patterns, respectively, a_i is the complex amplitude associated with path i, $e^{jkd_i(t)}$ is the corresponding distance-induced phase shift and $k = 2\pi\lambda^{-1}$ is the wave number. We can thus easily obtain the channel coefficients for different spatial subchannels of a MIMO system by summing up all our channel contributions according to (8) at the respective antenna elements, using the appropriate antenna patterns [29]. Furthermore, the "standard" single antenna impulse response is clearly a special case of the above formulation.

In agreement with our measurement results, we divide the impulse response of (8) into four parts: (i) the LOS component, which may contain more than just the true LOS signal, e.g., ground reflections, (ii) discrete components stemming from reflections off mobile scatterers[6] (MD), (iii) discrete components stemming from reflections off static scatterers (SD) and (iv) diffuse components (DI). We thus have (omitting the AOA and AOD notation for convenience):

$$h(t, \tau) = h_{\text{LOS}}(t, \tau) + \sum_{p=1}^{P} h_{\text{MD}}(t, \tau_p)$$
$$+ \sum_{q=1}^{Q} h_{\text{SD}}(t, \tau_q) + \sum_{r=1}^{R} h_{\text{DI}}(t, \tau_r), \quad (9)$$

where P is the number of mobile discrete scatterers, Q is the number of mobile static scatterers and R is the number of diffuse scatterers. Since the vast majority of the discrete components identified in the measurements are due to a single bounce, we assume such processes only[7] and hence the time-varying propagation distance $d(t)$ of each path is immediately given by the geometry. Furthermore, based on our observations in Sec. III-C, we assume that the complex path amplitude of the LOS path as well as the *discrete* scatterers is fading, i.e., $a_{\text{LOS}} = a_{\text{LOS}}(d)$, $a_p = a_p(d)$ and $a_q = a_q(d)$, which is in contrast to conventional GSCM modeling. This approach is thus a means of representing the combined contribution from several unresolvable paths by a single one, and we thus do all our (geometric) modeling in two dimensions only. The complex amplitudes of the diffuse scattering points are modeled as in standard GSCM, as will be discussed in the subsequent sections.

---

[6]Note that usage of the word "scatterer" is a slight abuse of notation, since the discrete components are not due to scattering, but rather "interaction" with objects.

[7]This assumption is also reasonable given the fairly low discrete scatterer density of our measurements. For denser environments, it is entirely possible that higher order reflections would have to be considered as well.
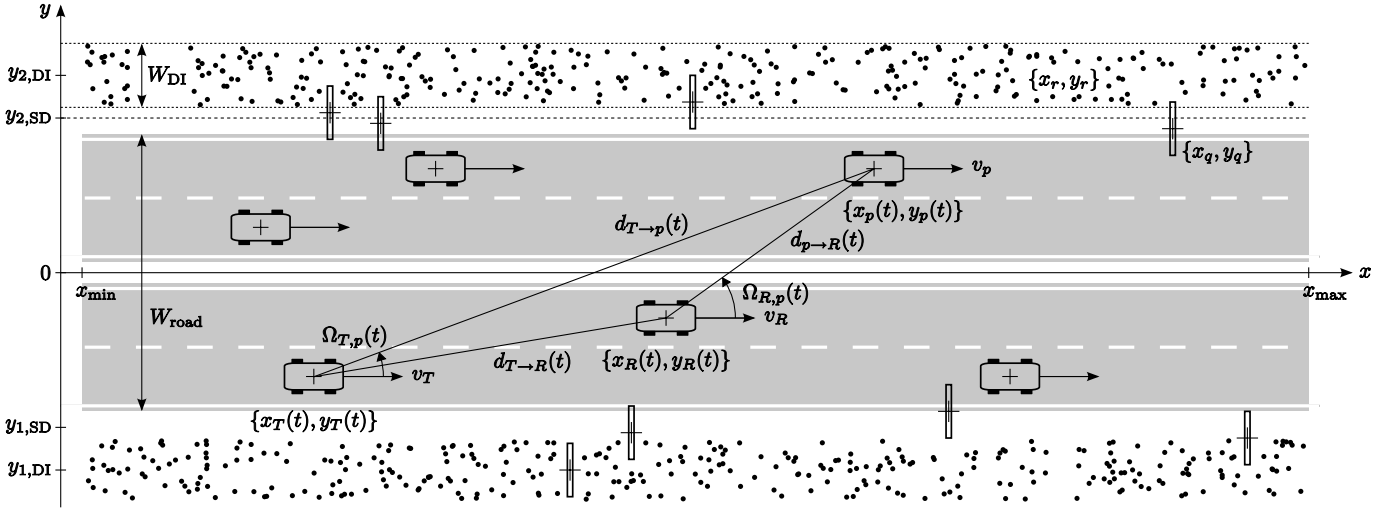
Fig. 7.　Geometry for the VTV channel model. A transmitter with (time-varying) coordinates $\{x_T(t), y_T(t)\}$, moving at a speed v_T in the direction of the x–axis, is communicating with a receiver with coordinates $\{x_R(t), y_R(t)\}$, moving at a speed v_R also in the direction of the x–axis. Scatterers are present as three types: mobile discrete scatterers (other vehicles) with coordinates $\{x_p(t), y_p(t)\}$ and a speed v_p, static discrete scatterers (road signs and other significant scattering points; visually represented by road signs) with coordinates $\{x_q, y_q\}$ and (static) diffuse scatterers (represented by dots) with coordinates $\{x_r, y_r\}$. The (time-varying) geometric relations between TX, RX and a mobile scatterer are also given in the figure (cf. (1)).

B. Scatterer Distributions

First, we let the number of point scatterers of each type be given by a density χ_{MD}, χ_{SD} and χ_{DI}, respectively, stating the number of scatterers per meter. Then, using the geometry in Fig. 7, we model the y–coordinate of mobile discrete scatterers by a uniform discrete probability density function (PDF) where the possible number of outcomes equals the number of road lanes, N_{lanes}. Their *initial* x–coordinates are modeled by a (continuous) uniform distribution over the length of the road strip, i.e., $x_{p,0} \sim \mathcal{U}[x_{min}, x_{max}]$. Each mobile scatterer is assigned a constant velocity along the x–axis given by a truncated Gaussian distribution (to avoid negative velocities in the wrong lane as well as too high velocities). We thus use a simplified model for the distribution of the discrete mobile scatterers; note, however, that our generic model can easily incorporate more complicated traffic models.

The x–coordinates of static discrete scatterers as well as diffuse scatterers are also modeled through $x_q \sim \mathcal{U}[x_{min}, x_{max}]$ and $x_r \sim \mathcal{U}[x_{min}, x_{max}]$. To model static discrete scatterers at either side of the road, we split the number of scatterers in two and derive separate y–coordinates for each side using Gaussian distributions $y_q \sim \mathcal{N}(y_{1,SD}, \sigma_{y,SD})$ or $y_q \sim \mathcal{N}(y_{2,SD}, \sigma_{y,SD})$, respectively (note that static scatterers in the middle of the road correspond to overhead road signs). Diffuse scatterers are also modeled on each side of the road strip; their y–coordinates are drawn from uniform distributions, over the intervals $y_r \sim \mathcal{U}[y_{1,DI} - W_{DI}/2, y_{1,DI} + W_{DI}/2]$ or $y_r \sim \mathcal{U}[y_{2,DI} - W_{DI}/2, y_{2,DI} + W_{DI}/2]$, where W_{DI} is the width of the scatterer field.

C. Discrete Scatterer Amplitude

We model the complex path amplitudes of the discrete scatterers as fading, thus representing the combined contributions of several (unresolvable) paths by a single process. We find it suitable to divide the complex amplitude a_p of a discrete component p into a deterministic (distance-decaying) part and a stochastic part, i.e.,

$$a_p(d_p) = g_{S,p} e^{j\phi_p} G_{0,p}^{1/2} \left(\frac{d_{ref}}{d_p} \right)^{n_p/2}, \qquad (10)$$

where $d_p = d_{T \to p} + d_{p \to R}$, $G_{0,p}$ is the received power at a reference distance d_{ref}, n_p is the pathloss exponent and $g_{S,p}$ is the real-valued, slowly varying,[8] stochastic amplitude gain of the scatterer (note that this representation is similar to the classical model for (narrowband) pathloss [29]); each discrete scatterer is assigned its own values for n_p, $G_{0,p}$. We stress that even though the model is the same for mobile and static scatterers, we provide separate sets of model parameters for each.[9]

The phase of the complex amplitude is obtained from the measured data by subtracting the distance-induced phase shift, $\exp\{-jkd_p\}$, from the discrete signal. Finding that the phase is only *slowly* varying, we subscribe this effect to phase drift of the TX/RX oscillators and noise and hence leave out any stochastic phase modeling. We instead follow the classical GSCM approach of giving the discrete scatterers a random phase shift, uniform over $[0, 2\pi)$.

The amplitude gain, $g_{S,p}$, is estimated by low-pass filtering $|a_p|^2$ by means of a sliding-average (a window size of 20 wavelengths was used), and then subtracting the distance-dependence as derived by simple regression analysis on the low-pass filtered signal. The distance dependence estimation is done through a fit to

$$G(d_p) = G_{0,p} - 10 n_p \log_{10} \left(\frac{d_p}{d_{ref}} \right), \qquad (11)$$

---

[8] A closer look at Fig. 6 suggests the existence of two random processes, one slow and one fast, though the variations of the fast fluctuations are small. However, since the total signal may contain estimation errors from the search-and-subtract algorithm, noise and fading produced by antenna vibration in conjunction with close scatterers surrounding it (the latter effect being confirmed as the dominating one through simulations), we deem the fast fluctuations of the signal highly specific for our measurement setup and choose not to include them in our model.

[9] In the extraction process, distinctions between reflections stemming from mobile objects and those stemming from static objects are made by examining their respective Doppler shifts; see Sec. III-B.
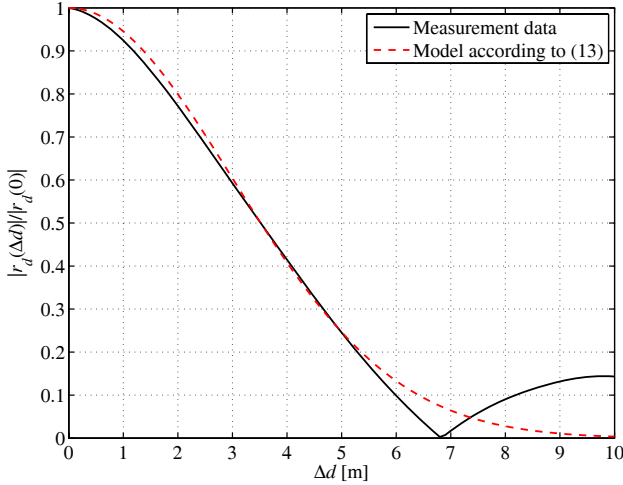
Fig. 8. Large-scale distance autocorrelation for the path denoted "19" in Fig. 5 plotted with a fit to (13).

i.e., a classical power law with a propagation exponent n_p. In the estimation process, we bound the range of possible outcomes to $0 < n_p < \infty$ and $P_{\text{noise-floor}} < G_{0,p} < G_{0,\text{LOS}}$, where $P_{\text{noise-floor}}$ is the noise floor power level and $G_{0,\text{LOS}}$ is the reference power of the LOS path, in order to obtain physical results (allowing $n_p < 0$ or $G_{0,p} > G_{0,\text{LOS}}$ leads to the undesirable effect of simulated reflected paths possibly carrying more power than the LOS path).

Since the distance-dependent mean of the total path gain has been removed, we make the simplifying assumption that $g_{S,p}$ can be treated as stationary. Finding $G_{S,p} = 20 \log_{10} g_{S,p}$ to be well described by a correlated Gaussian variable, i.e., $g_{S,p}$ is a correlated log-normal variable, we hence analyze its distance autocorrelation function

$$r_d (\Delta d) = E \{G_{S,p} G_{S,p}(d + \Delta d)\} . \qquad (12)$$

A commonly used model for describing large-scale fading is the exponential auto-correlation function [30]. Our estimated autocorrelation, however, is not well described by an exponential decay, especially around $\Delta d = 0$ (see Fig. 8). To obtain a better fit, we instead model it by means of another simple decaying function, the Gaussian function given by

$$r_d (\Delta d) = \sigma_S^2 e^{-\frac{\ln 2}{d_c^2}(\Delta d)^2}, \qquad (13)$$

where σ_S^2 is the variance of the process and d_c is the $0.5-$coherence distance defined by $\rho_d (d_c) = 0.5$. Separate values of $\sigma_{S,p}^2$ and $d_{c,p}$ are thus assigned to each discrete scatterer p.

D. LOS Amplitude

The tracked LOS components also show fading characteristics, likely due to the ground reflection which cannot be resolved from the true LOS. For this reason, we choose the same model for the LOS component as for the discrete components, i.e., we use (10) with the the subindex p replaced by LOS. In free-space, the pure LOS component would have $n_{\text{LOS}} = 2$, but the observed fading obviously opens up for other values as well. Again, we bound the range of valid n_{LOS} outcomes in the extraction process to positive values

only. Note that the model parameters for LOS are extracted first as they serve as input for the extraction of the discrete scatterer parameters.[10]

E. Diffuse Scatterer Amplitude

The complex path amplitude of a diffuse scatterer r is modeled as in classical GSCM by

$$a_r = G_{0,\text{DI}}^{1/2} c_r \left(\frac{d_{\text{ref}}}{d_{T \to r} \times d_{r \to R}} \right)^{n_{\text{DI}}/2}, \qquad (14)$$

where c_r is zero-mean complex Gaussian distributed in agreement with our observations in Sec. III-A. The pathloss exponent n_{DI} and the reference power $G_{0,\text{DI}}$ are the same for all diffuse scatterers.

Our tracking algorithm only provides information about discrete scatterers and does hence not directly provide information about n_{DI} and $G_{0,\text{DI}}$. However, these parameter can be estimated by means of simulations. First, "diffuse" impulse responses are derived from the measurement data by subtracting the LOS component and the discrete components detected by the tracking algorithm of Sec. III-C. Then the rms delay spread of the measured "diffuse" channel is determined as a comparative measure. By comparing these delay spreads to those obtained from simulations according to our model, best-fit values of n_{DI} and $G_{0,\text{DI}}$ can be estimated. Due to the randomness of the measured roadside environment, the extracted delay spreads vary within each measurement. Since such variations are not included in our model, we select the values of n_{DI} and $G_{0,\text{DI}}$ that provide the best fit *on average*. This approach is similar in spirit to [31], which also extracts discrete scatterers by high-resolution algorithms, and models the remainder as diffuse components whose PDF (in the delay/angle plane) is fixed, and whose parameters are extracted from best-fit.

F. Model Parameter Statistics

Our model requires the following signal model parameters: pathloss exponent n and reference power G_0 for the LOS component and all scatterers, and additionally a large-scale variance σ_S^2 and coherence distance d_c for the amplitude gain of the LOS component and the discrete scatterers. By extracting the parameters of all relevant paths using all available measurement data, we get an ensemble of results for each model parameter. Note that not all paths generated by the tracking algorithm are relevant, i.e., suitable for extracting distance-dependent parameters due to the short distance range over which they exist. In this paper, we have restricted the analysis to include only paths spanning over a relative distance range $2 (d_{\text{max}} - d_{\text{min}}) / (d_{\text{max}} + d_{\text{min}}) > 0.2$. Furthermore, out of the 16 antenna subchannels we have at our disposal, the parameters of (10) are only estimated from the channel

---

[10]In the post-processing, it was discovered that the LOS component of the SM highway measurements was approximately 20 dB lower than that of the other scenarios, likely due to the unintentional use of an additional attenuator during those measurements. Since this only affects the absolute power level, i.e., not the time-varying power fluctuations of a single component, we still include this scenario in the model parameter extraction process, though we exclude it from the extraction of n and G_0 for both discrete scatterers and the LOS component. Thus, for the highway scenario those model parameters are solely based on OP measurements.
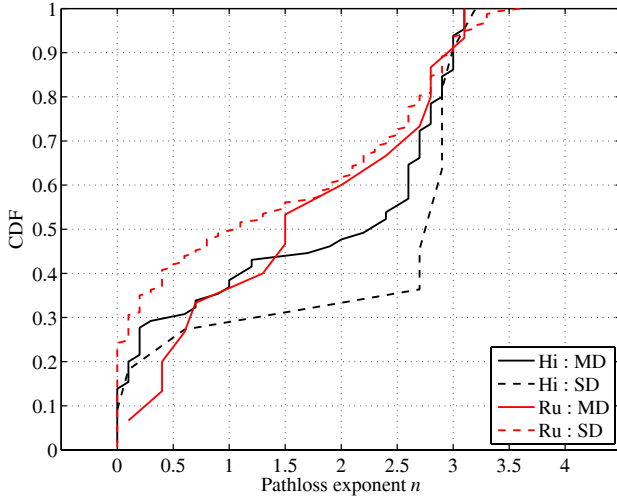
Fig. 9. CDF of the pathloss exponent n for the discrete components of the measured scenarios.
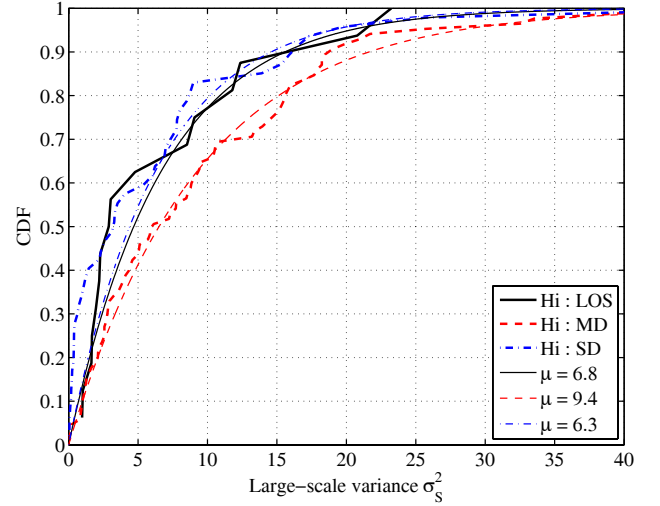

Fig. 10. CDF of the path gain variance for the LOS and discrete components of the highway scenario. The figure also shows exponential fits to each parameter set.

where the discrete component is strongest. With the distance ranges over which we observe the components, the changes in angles-of-arrival and departure are usually small enough to stay within the antenna 3 dB beamwidth and we thus make the assumption of a constant antenna gain over the duration of the observation.

Figs. 9 and 10 show cumulative distribution functions (CDFs) of two model parameters for the highway scenario (due to space limitations, we are prevented from showing all parameters). Based on the empirical CDFs, we find the following parameter models suitable:

- The **pathloss exponent** n is fixed for the LOS component (selected as the ensemble median value) and the diffuse scatterers. For discrete scatterers, $n \sim \mathcal{U}(0, n_{\max})$.
- The **reference power** G_0 of the discrete scatterers shows a high correlation with the pathloss exponent (~ 0.98), and is therefore modeled as a *function* of n. $G_{0,\text{DI}}$ and $G_{0,\text{LOS}}$ are fixed.
- The **coherence distance** d_c of the stochastic amplitude gain is given by an exponential distribution, though with a non-zero lowest value, i.e., $d_c = d_c^{\min} + d_c^{\text{rand}}$, where d_c^{rand} has a PDF $\mu_c \exp\{-\mu_c d_c\}$.
- The **variance** σ_S^2 of the stochastic amplitude gain is uncorrelated with d_c, and given by an exponential distribution with a PDF $\mu_\sigma \exp\{-\mu_\sigma \sigma_S^2\}$.

All model parameters are given in Table I.

V. IMPLEMENTATION RECIPE

The simulation procedure of the VTV GSCM can be summarized as follows:

1) Specify the physical limits of the geometry $\{x_{\min}, x_{\max}\}$, and determine the number of MD scatterers P, SD scatterers Q and DI scatterers R from their respective densities χ in Table I. Specify the simulation time frame and temporal resolution as well as frequency range and resolution. Specify the number of antennas in the MIMO system, their relative positions and antenna patterns.

TABLE I
MODEL PARAMETERS

	Parameter	Unit	LOS	MD	SD	DI
	G_0	dB	-5	$-89 + 24n$		104
	n		1.8	$\mathcal{U}[0, 3.5]$		5.4
	μ_σ		6.8	9.4	6.3	$-$
	μ_c	m	7.2	5.4	4.9	$-$
	$d_c^{\min}$	m	4.4	1.1	1.0	$-$
Hi	χ	m^{-1}	$-$	0.005	0.005	1
	y_1	m	$-$	$-$	-13.5	-13.5
	y_2	m	$-$	$-$	13.5	13.5
	W_{DI}	m	$-$	$-$	$-$	5
	W_{road}	m		18		
	N_{lanes}			4		
	G_0	dB	-9	$-89 + 24n$		23
	n		1.6	$\mathcal{U}[0, 3.5]$		3.0
	μ_σ		11.7	15.1	14.8	$-$
	μ_c	m	8.0	8.3	2.5	$-$
	$d_c^{\min}$	m	5.4	2.5	1.4	$-$
Ru	χ	m^{-1}	$-$	0.001	0.05	1
	y_1	m	$-$	$-$	-9.5	-9.5
	y_2	m	$-$	$-$	9.5	9.5
	W_{DI}	m	$-$	$-$	$-$	5
	W_{road}	m		8		
	N_{lanes}			2		

2) For each TX or RX antenna element, specify the initial position and determine their respective positions over the whole time frame. Specify velocity vectors for the TX and RX arrays. Generate initial coordinates and velocity for each MD scatterer according to Sec. IV-B, then determine their respective positions over the whole time frame. Generate coordinates for the SD and DI scatterers according to Sec. IV-B.

3) For every time instant, calculate the propagation distance, AOA and AOD for the LOS path as well as the single-bounce path from TX to RX via each scatterer.

4) Derive the zero-mean complex Gaussian amplitude c_r for each DI scatterer. For each MD or SD scatterer, derive its phase ϕ_p, pathloss exponent n_p, reference power $G_{0,p}$ and parameters for the large-scale fading of the amplitude gain, $\sigma_{S,r}^2$ and $d_{0.5,r}$. The path gain $g_{S,p}$

(or $g_{S,q}$) is generated by correlating uncorrelated (dB) data generated from $\mathcal{N}(0,1)$ using the autocorrelation function of (13) (e.g., by using a discrete linear filter, the covariance matrix or an auto-regressive process). Finally, generate the full complex amplitude for each of the LOS, MD and SD paths according to (10).

5) For each time sample and each antenna element, sum up all contributions at the RX according to (8) (applying the appropriate antenna pattern). Note that a band limited system implies a summation of *sinc* pulses instead of *Dirac* pulses.[11]

VI. COMPARISON WITH MEASUREMENTS

The validity of the model is examined by means of comparing extensive model simulations with the measurement data. Firstly, we note, by studying the simulation outputs in the time-delay domain and the delay-Doppler, that the suggested approach is well suited for SISO modeling; the (non-stationary) channel characteristics discussed in Sec. III are well captured (space reasons restrict us from showing this visually). Secondly, and more importantly, we want to verify the ability of the suggested model to represent quantities that were not an input to the model parameterization. This is done using the measured and modeled MIMO antenna correlation, i.e., we evaluate the complex correlation coefficient, defined for two complex random variables u and v as

$$\rho = \frac{E\left[uv^*\right] - E\left[u\right]E\left[v^*\right]}{\sqrt{\left(E\left[|u|^2\right] - |E\left[u\right]|^2\right)\left(E\left[|v|^2\right] - |E\left[v\right]|^2\right)}}, \quad (15)$$

where $(\cdot)^*$ denotes complex conjugation, between every two antenna subchannels. Again, we find the overall performance of the model satisfactory. We also note that the model outcome can vary a lot from one simulation to another; the latter being due to the non-stationary nature of the channel. More precisely, the correlation outcome depends largely on the strength and position of the discrete scatterers. This complicates giving an exact measure of the agreement between measurement and model as, in this aspect, the number of measurements to our disposal is relatively small. We instead settle for showing a typical comparison plot, as displayed in Fig. 11 where a simulation of a SD rural scenario is compared to a measurement with the same TX/RX speed and TX-RX separation.

Since the measured correlation values are affected by measurement noise, the best agreement between simulation outcomes and measurement results is obtained if also the simulations include the addition of white Gaussian noise (of the appropriate magnitude); a similar effect is discussed in [32]. Apart from that, deviations between measurement and model are largely explained by the simplifications of reality we use in our model:

- The diffuse scatterer distribution we use in the model is uniform with a constant density over the road strip, which is a major simplification of reality where some roadside sections were empty (e.g., fields) whereas other where heavily crowded with scatterers (e.g., highway exits).

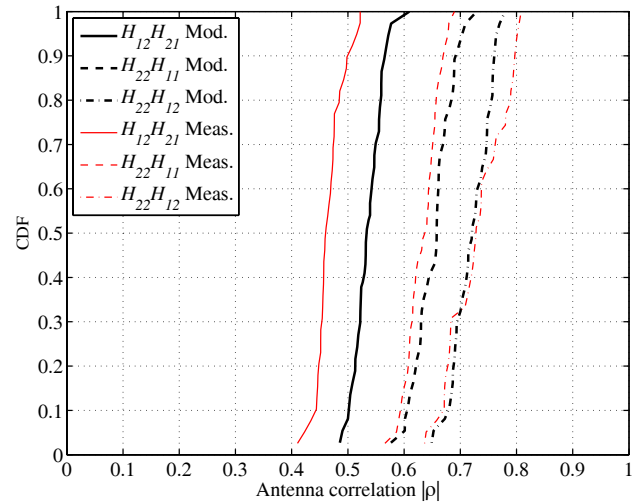[11]Alternatively, the calculations can be performed in the frequency domain.

Fig. 11. CDFs of measured and simulated antenna correlation for a time window of 3 s of a SM rural measurement with $v_T = v_R = 50$ km/h and $d_{T \to R} = 100$ m. H_{ij} defines the antenna subchannel from TX element j to RX element i and antenna elements 1 and 2 have their broadside directions at 135 and 45 degrees, respectively (see Sec. II-A).

- The TX and RX antenna patterns we use in the model simulations stem from calibration measurements of the arrays only, i.e., without the influence of the cars. This obvious simplification should imply a slightly higher simulated antenna correlation since we thus exclude the local scattering from the truck platforms.
- The highway section used for measurements contains a concrete barrier (approximately 0.5 m high) separating the directions of travel, which was not included in the model.
- The spatial distributions of the discrete scatterers are greatly simplified. The given scatterer densities are based on counting the number of visible scatterers along the measured road strips (for static scatterers) or coarse traffic statistics (which is available as an average over 24 hours only; for mobile scatterers) in conjunction with the number of observed echoes in the measurement data.

VII. SUMMARY AND CONCLUSIONS

We have presented a model that is suitable to describe the time-varying properties of a MIMO vehicle-to-vehicle propagation channel. The model is based on extensive measurements in highway and rural environments, from which we drew the following conclusions regarding the most significant and important contributors to the total signal:

- Apart from the LOS, significant energy is available from scatterers such as cars, houses and road signs on and next to the road. The contributions from these scatterers, labeled *discrete*, typically move through many delay bins during a measurement, thus violating the commonly adopted WSSUS assumption. Furthermore, their time-varying power is fading, likely due to the combination of the direct path with one or several ground-reflected paths.
- The LOS component is also fading, for the same reasons as above.

- The LOS is usually followed by a tail of weaker components, labeled *diffuse*, who give rise to Rayleigh distributed amplitude statistics in the delay bins immediately following the LOS.
- The total Doppler spread of the channel is large and the Doppler spectrum can change rapidly with time.

These conclusions suggest a need for a channel model capable of handling the non-WSSUS conditions typically arising in traffic environments. In order to capture the essentials of the measured channel though still keeping the model simple enough to be tractable for use, we found a geometry-based stochastic channel model (GSCM) as best suited.

Based on our measurement observations, we divided the impulse response of the model into four parts: LOS, discrete components stemming from interaction with mobile objects, discrete components stemming from interaction with static objects, and diffuse scattering and gave a detailed description for each. The key points are summarized as follows:

- Diffuse scatterers are modeled as in classical GSCM, i.e., with random complex Gaussian amplitudes, but to obtain the correct Doppler spread, these scatterers are only located in two bands, on either side of the road.
- In contrast to classical GSCM, the amplitude of the LOS and the discrete scatterers is modeled as fading; this is included by means of a distance-dependent decay in conjunction with a large-scale stochastic process. The corresponding phase is uniformly distributed.
- All scattering is assumed to be single-bounce only.

Model parameters were extracted from all available measurement data using a high resolution algorithm (for signal parameters) and the measurement environment (for geometry parameters) and given as constants or statistical distributions. We gave the full model parameterization and included a complete implementation recipe. Finally, simulations of the model were performed and compared to the measurement data. We noted that the model is well capable of representing the SISO as well as MIMO characteristics of the measured vehicle-to-vehicle channel though simplifications made in the modeling approach (concerning the scattering process, the antenna patterns and the scatterer distributions) are expected to induce minor differences between model and measurements. We thus conclude that the model gives a good overall description of the MIMO VTV channel and can be used for simulations of future wireless systems.

ACKNOWLEDGMENTS

REFERENCES

[1] J. Zhu and S. Roy, "MAC for dedicated short range communications in intelligent transport systems," *IEEE Commun. Mag.*, vol. 41, no. 12, pp. 60–67, Dec. 2003.
[2] IEEE Draft Standard IEEE P802.11p/D0.26 Jan. 2006, "Draft amendment to standard for information technology telecommunications and information exchange between systems local and metropolitan networks; specific requirements part 11: Wireless LAN medium access control (MAC) and physical layer (PHY) specifications amendment 3: Wireless access in vehicular environments (WAVE)," Tech. Rep., 2006.
[3] J. H. Winters, "On the capacity of radio communications systems with diversity in Rayleigh fading environments," *IEEE J. Select. Areas Commun.*, vol. 5, no. 5, pp. 871–878, June 1987.
[4] G. J. Foschini and M. J. Gans, "On limits of wireless communications in a fading environment when using multiple antennas," *Wireless Personal Commun.*, vol. 6, pp. 311–335, Feb. 1998.
[5] A. Paier, J. Karedal, N. Czink, H. Hofstetter, C. Dumard, T. Zemen, F. Tufvesson, A. F. Molisch, and C. F. Mecklenbräuker, "First results from car-to-car and car-to-infrastructure radio channel measurements at 5.2 GHz," in *Proc. IEEE Int. Symp. Personal, Indoor, Mobile Radio Commun.*, vol. 1, 2007, pp. 1–5.
[6] H. Asplund, A. A. Glazunov, A. F. Molisch, K. I. Pedersen, and M. Steinbauer, "The COST259 directional channel model - II. macrocells," *IEEE Trans. Wireless Commun.*, vol. 5, pp. 3434–3450, 2006.
[7] P. Almers, E. Bonek, A. Burr, N. Czink, M. Debbah, V. Degli-Esposti, H. Hofstetter, P. Kyoesti, D. Laurenson, G. Matz, A. Molisch, C. Oestges, and H. Oezcelik, "Survey of channel and radio propagation models for wireless MIMO systems," *EURASIP J. Wireless Commun. Networking*, vol. 2007.
[8] J. Maurer, "Strahlenoptisches Kanalmodell für die Fahrzeug-Fahrzeug-Funkkommunikation," Ph.D. dissertation, Institut für Höchstfrequenztechnik und Elektronik (IHE), Universität Karlsruhe (TH), Karlsruhe, Germany, July 2005, in German.
[9] J. Maurer, T. Fugen, T. Schafer, and W. Wiesbeck, "A new inter-vehicle communications (IVC) channel model," in *Proc. IEEE Veh. Technol. Conf. 2004 Fall*, vol. 1, pp. 9–13, Sept. 2004.
[10] J. Maurer, T. Fugen, and W. Wiesbeck, "Narrow-band measurement and analysis of the inter-vehicle transmission channel at 5.2 GHz," in *Proc. IEEE Veh. Technol. Conf. 2002 Spring*, vol. 3, pp. 1274–1278, 2002.
[11] P. A. Bello, "Characterization of randomly time-variant linear channels," *IEEE Trans. Commun.*, vol. 11, pp. 360–393, 1963.
[12] A. F. Molisch and F. Tufvesson, "Multipath propagation models for broadband wireless systems," in *Digital Signal Processing for Wireless Communications Handbook*, M. Ibnkahla, ed. CRC Press, 2004.
[13] COST 207, "Digital land mobile radio communications," Office for Official Publications in European Communities, Tech. Rep., 1989, final report, Luxembourg.
[14] WINNER, "Final report on link level and system level channel models," Tech. Rep. IST-2003-507581, 2003.
[15] G. Acosta-Marum and M. A. Ingram, "Six time- and frequency-selective empirical channel models for vehicular wireless LANs," in *Proc. IEEE Veh. Technol. Conf. 2007 Fall*, Sept. 2007, pp. 2134–2138.
[16] G. Acosta-Marum and M. A. Ingram, "Doubly selective vehicle-to-vehicle channel measurements and modeling at 5.9 GHz," in *Proc. Int. Symp. Wireless Personal Multimedia Commun.*, 2006.
[17] G. Acosta-Marum and M. A. Ingram, "A BER-based partitioned model for a 2.4 GHz vehicle-to-vehicle expressway channel," *Wireless Personal Commun.*, vol. 37, no. 3, pp. 421–443, 2006.
[18] A. Paier, T. Zemen, L. Bernado, G. Matz, J. Karedal, N. Czink, C. Dumard, F. Tufvesson, A. F. Molisch, and C. F. Mecklenbräuker, "Non-WSSUS vehicular channel characterization in highway and urban scenarios at 5.2 GHz using the local scattering function," in *International ITG Workshop on Smart Antennas*, 2008.
[19] J. Fuhl, A. F. Molisch, and E. Bonek, "Unified channel model for mobile radio systems with smart antennas," in *IEE Proc. Radar, Sonar Navig.*, vol. 145, Feb. 1998, pp. 32–41.
[20] P. Petrus, J. H. Reed, and T. S. Rappaport, "Geometrical-based statistical macrocell channel model for mobile environments," *IEEE Trans. Commun.*, vol. 50, pp. 495–502, 2002.
[21] A. F. Molisch, A. Kuchar, J. Laurila, K. Hugl, and R. Schmalenberger, "Geometry-based directional model for mobile radio channels-principles and implementation," *European Trans. Telecommun.*, vol. 14, pp. 351–359, 2003.
[22] A. F. Molisch, "A generic channel model for MIMO wireless propagation channels in macro- and microcells," *IEEE Trans. Signal Processing*, vol. 52, no. 1, pp. 61–71, Jan. 2004.
[23] M. Pätzold, B. rn Olav Hogstad, and N. Youssef, "Modeling, analysis, and simulation of MIMO mobile-to-mobile fading channels," *IEEE Trans. Wireless Commun.*, vol. 7, no. 2, pp. 510–520, Feb. 2008.
[24] A. G. Zajić and G. L. Stüber, "Three-dimensional modeling, simulation, and capacity analysis of spacetime correlated mobile-to-mobile channels," *IEEE Trans. Veh. Technol.*, vol. 57, no. 4, pp. 2042–2054, July 2008.
[25] A. Paier, J. Karedal, N. Czink, H. Hofstetter, C. Dumard, T. Zemen, F. Tufvesson, A. F. Molisch, and C. F. Mecklenbräuker, "Car-to-car radio channel measurements at 5 GHz: Pathloss, power-delay profile, and delay-doppler spectrum," in *Proc. Int. Symp. Wireless Commun. Syst.*, 2007, pp. 224–228.

[26] R. Thomae, D. Hampicke, A. Richter, G. Sommerkorn, A. Schneider, U. Trautwein, and W. Wirnitzer, "Identification of the time-variant directional mobile radio channels," *IEEE Trans. Instrum. Meas.*, vol. 49, pp. 357–364, 2000.

[27] P. Hakansson, Lunds Kommun, 2008, private communications.

[28] R. J.-M. Cramer, R. A. Scholtz, and M. Z. Win, "Evaluation of an ultra-wide-band propagation channel," *IEEE Trans. Antennas Propagat.*, vol. 50, no. 5, pp. 541–550, May 2002.

[29] A. F. Molisch, *Wireless Communications*. Chichester, West Sussex, UK: IEEE Press–Wiley, 2005.

[30] M. Gudmundsson, "Correlation model for shadow fading in mobile radio systems," *IEEE Electron. Lett.*, vol. 27, no. 23, pp. 2145–2146, Nov. 1991.

[31] A. Richter, "Estimation of radio channel parameters: models and algorithms," Ph.D. dissertation, University of Ilmenau, Ilmenau, Germany, May 2005.

[32] M. Toeltsch, J. Laurila, K. Kalliola, A. F. Molisch, P. Vainikainen, and E. Bonek, "Statistical characterization of urban spatial radio channels," *IEEE J. Select. Areas Commun.*, vol. 20, pp. 539–549, Apr. 2002.

Johan Karedal received his M.S. degree in engineering physics in 2002 and his Ph.D. in radio communications in 2009, both from Lund University, Sweden. He is currently a researcher at the Department of Electrical and Information Technology, Lund University, where his main research interests concern measurements and modeling of the wireless propagation channel for MIMO and UWB systems. Dr. Karedal has participated in the European research initiative "MAGNET."

Fredrik Tufvesson was born in Lund, Sweden in 1970. He received the M.S. degree in Electrical Engineering in 1994, the Licentiate Degree in 1998 and his Ph.D. in 2000, all from Lund University in Sweden. After almost two years at a startup company, Fiberless Society, Fredrik is now associate professor at the Department of Electrical and Information Technology. His main research interests are channel measurements and modeling for wireless communication, including channels for both MIMO and UWB systems. Beside this, he also works with channel estimation and synchronization problems, OFDM system design and UWB transceiver design.

Nicolai Czink did his Dipl.-Ing. (M.S.) degree in 2004 and Dr.techn. (Ph.D.) degree in 2007, both at Vienna University of Technology, Austria, with distinction. His Ph.D. thesis received an award from the Austrian Electrotechnical Association (OVE). After his Ph.D., he joined Stanford University as a Postdoctoral Researcher on an Erwin Schrdinger Fellowship of the FWF Austrian Science Fund. He is currently Senior Researcher at the ftw. Telecommunications Research Center Vienna, Austria, working on channel modeling, cooperative communications, and intelligent transportation systems.

Alexander Paier received his Dipl.-Ing. (M.S.) degree in electrical engineering from the Vienna University of Technology, Austria, in 2006. Since July 2006 he is working as research assistant on his doctoral thesis at the Institute of Communications and Radio-Frequency Engineering at the Vienna University of Technology. He participates in the COST Action 2100 "Pervasive Mobile and Ambient Wireless Communications." His current research interests focus on channel sounding and modeling for vehicular communication networks.

Thomas Zemen was born in Mödling, Austria in 1970. He received the Dipl.-Ing. degree (with distinction) in electrical engineering from Vienna University of Technology in 1998 and the doctoral degree (with distinction) in 2004. He joined Siemens Austria in 1998 where he engaged in the development of a vehicular communication system for a German car manufacturer. Since October 2003 Thomas Zemen has been with the Telecommunications Research Centre Vienna. Since 2008 Thomas Zemen holds a key researcher position at FTW and leads the research area "Signal and Information Processing." He manages the project "Cooperative Communications for TrafficTelematics" and is the speaker of the national research network for "Signal and Information Processing in Science and Engineering." Dr. Zemen teaches "Cooperative Communications" as external lecturer at Vienna University of Technology. He has authored or co-authored 2 book chapters, 8 journal papers and 47 conference papers.

Christoph F. Mecklenbräuker (S'88-M'97-SM'08) received the Dipl.-Ing. degree in electrical engineering from Technische Universität Wien, Austria, in 1992 and the Dr.-Ing. degree from Ruhr-Universität Bochum, Germany, in 1998. He was with Siemens AG Austria during 1997–2000 and engaged in the standardization of the Universal Mobile Telecommunications System (UMTS). During 2000–2006, he was a senior researcher at the Forschungszentrum Telekommunikation Wien (ftw.) in Vienna, Austria. In 2006, he joined the Faculty of Electrical Engineering and Information Technology as a Full Professor with the Technische Universität Wien, Austria. He has authored approximately 100 papers in international journals and conferences and holds eight patents in the field of mobile cellular networks. His current research interests include ultrawideband radio and MIMO-signal processing for vehicular wireless systems. Dr. Mecklenbräuker is a member of the IEEE Signal Processing, Antennas and Propagation, and Vehicular Technology Societies, and EURASIP.

Andreas F. Molisch (S'89, M'95, SM'00, F'05) is Professor of Electrical Engineering at the University of Southern California, Los Angeles, CA, USA. Previously, he was with AT&T (Bell) Laboratories Research (USA), Mitsubishi Electric Research Labs, (USA), TU Vienna (Austria), and Lund University (Sweden).

Dr. Molisch's current research interests are measurement and modeling of mobile radio channels, UWB, cooperative communications, and MIMO systems. He has authored, co-authored or edited four books (among them the textbook *Wireless Communications*, Wiley-IEEE Press), eleven book chapters, more than 110 journal papers, and numerous conference contributions, as well as more than 70 patents.

Dr. Molisch has been an editor of a number of journals and special issues, General Chair, TPC Chair, or Symposium Chair of multiple international conferences, and chairman of various international standardization groups. He is a Fellow of the IEEE, a Fellow of the IET, an IEEE Distinguished Lecturer, and recipient of several awards.